Indian Journal of Pure & Applied Physics
Vol. 60, February 2022, pp. 138-149

Structural and Optoelectronic Characterization of Synthesized Undoped CZTS and Cd-doped CZTS Thin Films

A B Migdadi, F Y Alzoubi*, H M Al-Khateeb & M K Alqadi
Department of Physical Sciences, Jordan University of Science & Technology, P.O. Box 3030, Irbid-22110, Jordan

Received 4 September 2021; accepted 14 January 2022

Copper zinc tin sulfide (CZTS) thin films with different doping ratios of Cadmium (Cd) were successfully fabricated using the sol-gel method by dip-coating technique. The surface morphology, the crystal structure properties as well the optical properties of undoped CZTS thin film and Cd- doped CZTS thin films were investigated using scanning electron microscopy (SEM), x-ray diffraction (XRD), and UV-Vis spectrophotometer. SEM micrographs demonstrated that the size and morphology of the particles improve due to increasing the Cd concentration in CZTS thin films. In addition, the XRD patterns exhibited the crystalline nature for CZTS thin films with kesterite crystal structure and showed improvement in some crystal structure properties such as crystal size and volume of unit cell with the incorporation of Cd into CZTS thin films. Moreover, optical bandgap energy E_g, in addition to several optoelectronic parameters such as refractive index (n), extinction coefficient (k), dispersion energy, high-frequency dielectric constant, density of state, Plasma frequency, and relaxation time have been estimated. Remarkably, the bandgap energy of CZTS thin films ranges from 1.594 eV to 1.529 eV depending on the Cd content; it increases with increases the concentration of Cd into CZTS thin films.

Keywords: CZTS thin film; Cd-doped CZTS; sol-gel method; density of state; dispersion parameters; high-frequency dielectric constant; Plasma frequency; relaxation time

1 Introduction

Cu_2ZnSnS_4 (copper zinc tin sulfide or CZTS) thin films are considered one of the most promising materials which have been studied well during the past decade for thin films solar cells applications as an absorber layer[1-3]. CZTS is a p-type semiconductor material and has an ideal optical direct bandgap energy between 1.45 eV and 1.6 eV with high absorption coefficient over 10^{-4} cm^{-1} in addition to a crystal structure of kesterite (KS) that belongs to the tetragonal system[3-5]. CZTS thin films have a similar structure and optical properties similar to some rare and expensive semiconductor materials used in thin film solar cell applications such as $CuGaSe_2$, $CuInSe_2$, and $Cu(Ga, In)Se_2$. However, CTZS is characterized by its abundance in nature as well as it is considered friendly to the environment[6-8]. There are various physical and chemical techniques that have been used to fabricate CZTS thin films like pulsed laser deposition[9], evaporation[10], sputtering[11], spray deposition[12], chemical bath deposition[13], electrodeposition[14] and sol-gel method[15,16].

The experimental efficiency of CZTS thin film solar cells is about 12%, but the expected theoretical efficiency is about 32% due to their interesting optical and electrical properties[6,17,18]. Therefore, there are many researchers have tried to enhance the optical, structural, and electrical properties of CZTS thin films to achieve higher possible efficiency of absorber layers by different strategies like replacing S atoms with Se atoms[19,20] and replacing Zn atoms with one of the transition elements such as Fe[21], Cr [18,22] and Co[20], also, using additional elements in the CZTS thin films by doping with some element like Ag [23], Na[24], Mg[25], Cr[26] and Bi[27]. These strategies will lead to optical band gap tuning and improving the crystal structure that have a significant role in improving the efficiency of the CZTS thin films solar cells[28]. The results of replacing atoms lead to a change in the effective ionic radius of atoms. In contrast, the increasing or decreasing atoms will lead to a change in the structural and optical properties of thin films[18].

The objective of this study is to examine the effect of Cd atoms comprehensively on the crystal structure parameters and optical properties for CZTS thin films. In this paper, undoped CZTS thin film and Cd-doped

*Corresponding author: (E-mail: fedda@just.edu.jo)

CZTS thin films were fabricated by the sol-gel method using the immersion method. In addition, structural, optical, and morphology properties of CZTS thin films were studied using X-ray diffraction (XRD), UV-Vis Spectroscopy, and scanning electron microscope (SEM).

2 Experimental Procedure

2.1. CZTS thin films synthesis

The CZTS solution was prepared using the sol-gel method and deposited on cleaned glass substrates by immersion to form CZTS thin films. The starting materials of CZTS solution are copper acetate dehydrates ($C_4H_{10}CuO_6.2H_2O$), zinc acetate dihydrate ($ZnC_4H_6O_4.2H_2O$), tin chloride ($SnCl_2$) and thiourea (CH_4N_2S), and 2-methoxyethanol ($C_3H_8O_2$) as a solvent, and Ethanolamine (C_2H_7NO) as stabilizer agent, in addition, the cadmium acetate dihydrate ($C_4H_6CdO_4.2H_2O$) used as a dopant agent to CZTS thin films.

4.78 g of copper acetate (0.26 M), 3 g of zinc acetate (0.14 M), 2.3 g of tin chloride (0.12 M), and 3.7 g of thiourea (0.48 M) were mixed and dissolved in 100 ml of the solvent. The solution was placed on a hot plate with stirring at 90 C for 3 h; when the mixture was dissolved entirely, Ethanolamine was added drop by drop to the mixture under continuous stirring and heating. The solution was left to cool down at room temperature; then, it was divided into 4 samples using glass beakers, each containing 25 ml of CZTS solution with different doping ratios of cadmium acetate (0 %, 1 %, 2 %, and 4 %).

The samples with cadmium acetate were stirred for 1h at room temperature to get a homogeneous solution of CZTS with different doping ratios. The glass substrates were cleaned by ethanol, acetone, and then deionized water and left to dry at room temperature. CZTS thin films were prepared by immersing the glass substrates vertically into the prepared solutions using 4 glass beakers for 2 h at room temperature to produce a one-layer of CZTS thin films. The glass substrates were taken away from the beakers and dried by a hot plate at 60 ^{o}C for about 40 min to evaporate the solvent and organic residues. Finally, the undoped CZTS thin film and Cd-doped CZTS thin films were annealed under N_2 atmosphere at 550 for 1 h to enhance the crystallinity of the CZTS thin films[29].

2.2. Characterization techniques

The surface morphology of undoped CZTS thin film and Cd-doped CZTS thin films were investigated using scanning electron microscopy (SEM, Quanta FEG 450). The crystalline nature and the crystal structure properties of the undoped CZTS thin film and Cd-doped CZTS thin films were investigated by a Powder X-Ray Diffraction (XRD, Rigaku Ultima IV) using monochromatic CuKα radiation with a wavelength of 0.1540598 nm at room temperature. The transmittance and reflectance spectra of thin films were investigated using a double-beam UV-Vis spectrophotometer (U-3900H).

3 Results and discussions

3.1. Surface morphology of CZTS thin films

Fig 1a-d shows the scanning electron micrographs that display the surface morphology of undoped CZTS thin film and (1 %, 2 %, 4 %) Cd-doped CZTS thin films. Generally, it is clear that the undoped and Cd-doped CZTS thin films contain tiny spherical particles with an average size in the nanoscale, and this indicates that CZTS thin films have a nanostructure. The size and morphology of the particles improve due to increasing the Cd concentration in CZTS thin films. Fig c and d demonstrates that the particles become clearer and larger. This behavior is consistent with the XRD analysis, where the 4 % Cd-doped CZTS have the largest crystal size. It's worth mentioning that the efficiency of absorber layers for CZTS thin film solar cells increases with increasing grains size that is required to improve the performance of photovoltaic devices [30,31].

The thickness of the CZTS thin films was estimated by cross-section SEM micrograph for undoped CZTS thin film as a standardized sample; the CZTS thin film was prepared to scan by cutting the glass substrate to the small pieces $(1cm \times 1cm)$, which may affect the accuracy of the film thickness measurement. Fig 2 shows the cross-section micrograph of undoped CZTS thin film, the thickness of CZTS thin film was found to be about 500 nm.

3.2. Structural properties of CZTS thin films

The crystal structural properties of CZTS thin films were analyzed using powder X-ray diffraction (XRD) in the range 2θ from 20° to 60°. Fig. 3 displays the XRD patterns of undoped CZTS and doped CZTS with different doping concentrations (1 %, 2 %, 4 %) of Cd. Four peaks located at the positions 2θ; 28°, 33.4°, 47°, and 55° were observed, and they are related to the crystal reflection planes (112), (200), (220), and (312), respectively, These peaks are

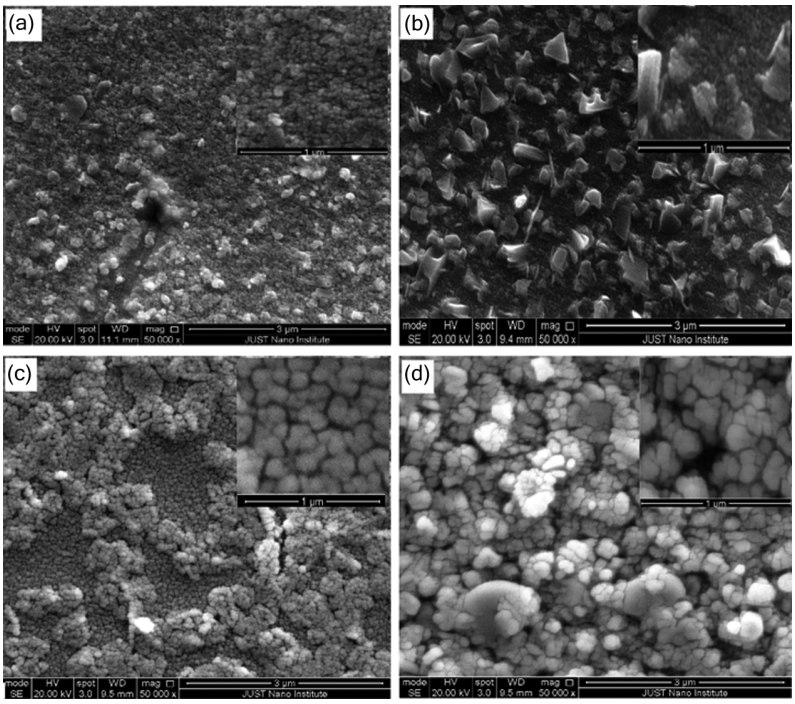

Fig. 1 — SEM micrographs of (a) undoped CZTS thin film and (b-d) Cd-doped CZTS thin films with (1%,2% and 4%) doping ratio, respectively.

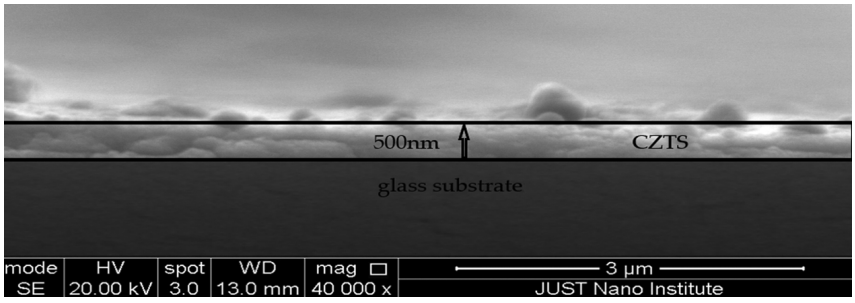

Fig. 2 — Cross- section SEM micrograph of undoped CZTS thin film.

attributed to the formation of CZTS with kesterite structure which belongs to the tetragonal system[32,33]. Two peaks belonging to the $ZnSO_3$ appear at 2θ values of 26.2° and 51° indicating the formation of another phase in the structure; these results agree with previous reports[33-35]. It is clear that the Cds phase started to appear clearly at the high concentration (4 %) of Cd dopant at 2θ values of 24.9°, 26.74°, 28.4°, 37.6°, 44.6°, and 48.76°, in agreement with what has been reported previously in the literature[36].

One may observe a slight shift in the position of the main peak (112) toward lower 2θ values, and this shift increases as the Cd concentration increases in CZTS thin films. Results of the (112) peak shift and other related parameters are listed in Table 1. The shift in the 2θ may be attributed to the increase in lattice plane space (d) value which may lead to an increase in the lattice parameters and the volume of

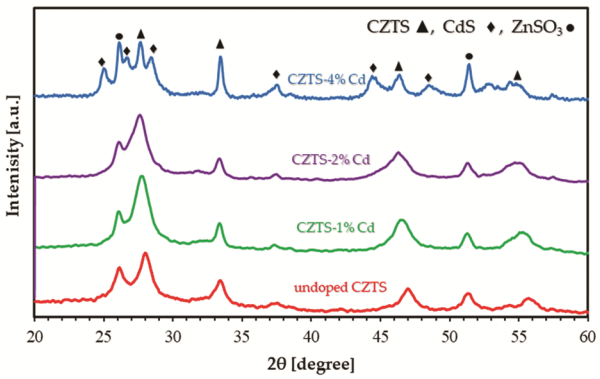

Fig. 3 — XRD pattern of undoped CZTS and doped CZTS with different concentrations (1%.2%,4%) of Cd.

the unit cell[18]. Some reports demonstrated that some Zn and Cu atoms sites are replaced by Cd atoms at the low and high doping concentration of Cd [5,28], thus increasing the (d) value leads to decreasing the

2θ values as the Cd concentration increased may occur because of the large effective ionic radius of Cd^{+2} compared to Cu^{+2} , Zn^{+2} as the small ions replaced with large ions, where it's worth mentioning that the effective ionic radius of Cd^{+2}, Cu^{+2} and Zn^{+2} and are 0.95 Å ,0.74 Å and 0.73 Å, respectively [6,18,28].

To examine the crystal structure parameters and figure out the effect of Cd atoms on the CZTS thin films, the lattice parameters (a = b) and c have been calculated using the following equation used for the tetragonal system [37].

$$\frac{1}{d^2} = \frac{h^2+k^2}{a^2} + \frac{l^2}{c^2} \quad \dots (1)$$

where d is the lattice plane space, which could be determined using Bragg's law ($\lambda = 2d_{hkl}\, sin\, sin\, \theta_{hkl}$) and (h,k,l) are the miller indices of the lattice planes.

Other important structural parameters such as volume of unit cell (V) and degree of crystal lattice distortion (R) were calculated using a^2c and $c/2a$, respectively[38]. Table 1 represents the crystal lattice parameters (a,c), the lattice plane (d), volume of unit cell (V) , and the degree of crystal lattice distortion (R) of undoped and doped CZTS thin films with different ratios of Cd.

The calculated value of the lattice plane space (d) was 3.18 Å for undoped CZTS thin film, which increased for Cd-doped CZTS thin films due to increasing the doping ratio. As a result of this increase, the lattice parameter (c) will increase; hence the volume of the unit cell and lattice distortion (R) as shown in table1, where the lattice parameters value of undoped CZTS was found to be $a = b$ = 5.34 Å and $c =$ 11.74 Å, the ideal value of a and c for powder CZTS are 5.43 Å and 10.84 Å, the difference may be attributed to the formation of another phase in the structure of $ZnSO_3$.

The volume of unit cells of undoped and doped CZTS thin films ranges from 334.7 Å^3 to 351 Å^3 the degree of crystal lattice distortion (R) of undoped CZTS thin film is 1.09. It increases up to be 1.146 for the high doping concentration (4%), indicating a slight distortion in the lattice structure which expresses the change in atoms positions from an ideal structure. Replacing small ions with large ions will result in an increase in the volume of the unit cell, as shown in Table1.

The crystal size (grain size) (D) and the microstrain (ε) of undoped and Cd-doped CZTS thin films were calculated using equation 2 (Debye Scherrer's equation) and equation 3, respectively[4,39].

$$D = \frac{\lambda K}{\beta cos\, \theta} \quad \dots (2)$$

$$\varepsilon = \frac{\beta cot\, \theta}{4} \quad \dots (3)$$

where D is the crystal size, ε is the microstrain, k is the constant equals 0.94, β is the full width at half maximum (FWHM) in radians, λ is the wavelength of the X-ray diffraction ($\lambda = 0.154184\, nm$), and θ is Bragg's angle at the peak position. The obtained values of the (D) and (ε) are tabulated in Table 2.

Table1 — The lattice parameters and inter planar spacing for undoped and Cd- doped CZTS thin films.

Samples	2θ [degree]	d (Å) (112)	a (Å)	c (Å)	a^2c (Å^3)	$c/2a$
Undoped CZTS	28.1	3.18	5.34	11.74	334.7	1.09
CZTS-1% Cd	27.8	3.2	5.35	11.94	341.75	1.11
CZTS-2% Cd	27.68	3.22	5.35	12.24	350	1.143
CZTS-4% Cd	27.66	3.23	5.35	12.27	351	1.146

Table 2 — the crystal size (grain size) (D),the microstrain (ε), the dislocation density (δ), the average of crystallites density (N), The total internal stress (σ) and the strain energy density (E_d) of undoped and Cd-doped CZTS thin films.

Samples	2θ [degree]	FWHM (112)	D [nm]	ε (10^{-2})	δ* (10^{12}) [lines/cm^2]	(N)*10^{14} [crys./cm^2]	$\sigma * 10^9$ $[N.m^{-2}]$	$E_d * 10^7$ $[J.m^{-3}]$
Undoped CZTS	28.1	1.53063	5.58	2.7	3.2	2.8	1.5	1.95
CZTS-1% Cd	27.8	1.47176	5.8	2.6	2.9	2.5	1.4	1.85
CZTS-2% Cd	27.68	1.35402	6.3	2.4	2.5	2	1.3	1.58
CZTS-4% Cd	27.66	0.88306	9.7	1.6	1.1	0.55	0.86	0.67

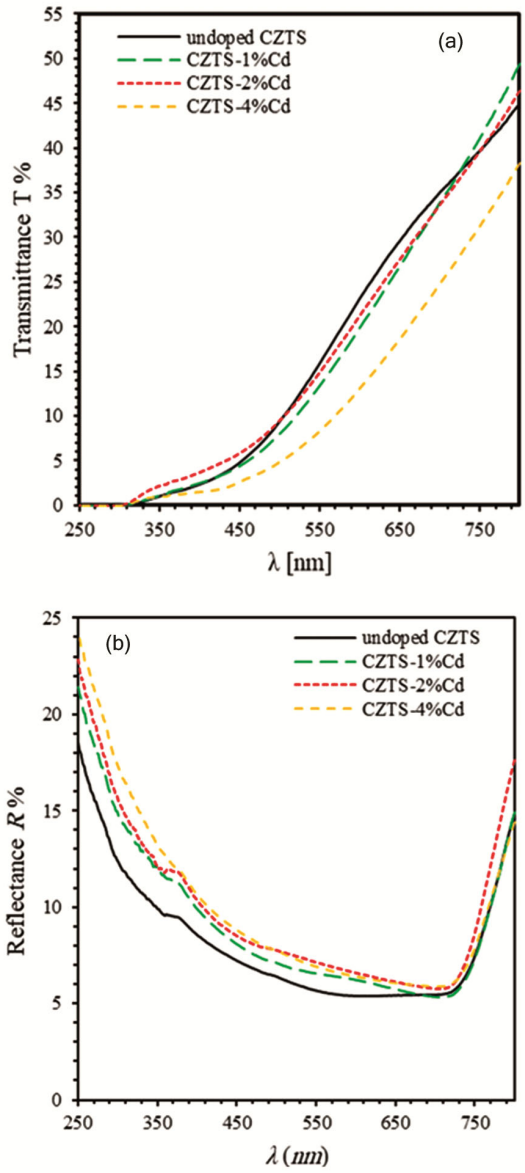

Fig. 4 — (a) Transmittance (T%) spectra, (b) Reflectance (R%) spectra of undoped and doped CZTS thin films.with different ratios of Cd.

It is clear that the average values of D increase as the Cd concentration increase in thin films while the average values of ε decrease. The D and ε values of undoped CZTS thin film were found to be 5.58 nm and 2.7 $*10^{-2}$, respectively.

Furthermore, the dislocation density (δ) and the average of crystallites density (N) of CZTS thin films have been evaluated by $\delta = \frac{1}{D^2}$ and $N = \frac{t}{D^3}$, respectively, where t is the thickness of thin-film[40].

The obtained values of the δ and N are listed in Table 2. The results of δ and N values present a decreasing behavior as the Cd concentration increase in CZTS thin films, where the high values of δ and N are for the undoped CZTS. This behavior enhances the lattice quality for CZTS thin films doped with Cd atoms.

The total internal stress (σ) and the strain energy density (E_d) can be calculated as follows $\sigma = E * \langle\varepsilon\rangle$ and $E_d = \frac{1}{2}E\langle\varepsilon\rangle^2$, respectively, where E is theoretical Young's Modulus, which is equal to 55 Gpa for CZTS [7,39]. The values of total internal stress (σ) and the strain energy density (E_d) of all thin films are tabulated in Table 2. The total internal stress (σ) and the strain energy density (E_d) decrease as the concentration of the Cd atoms increases in the CZTS thin films due to the reduction in the microstrain and the increase in the volume of the unit cell[41]. The decrease in the total internal stress and the strain energy density indicates the formation of CZTS thin films with less lattice defects[42].

3.3. Optical properties of CZTS thin films

Fig 4(a) and 4(b) show the transmittance (T%) and reflectance (R%) spectra in the wavelength range (250–800) nm of doped and undoped CZTS thin films. The spectra show almost zero transmittance below 350 nm however, when the wavelength exceeds 350 nm the transmittance increases rapidly. In general, the curves show a decrease in the transmittance as the concentration of Cd atoms increases in thin films.

The reflectance of undoped and doped CZTS thin films decreases in the wavelength from 250 nm to 700 nm, while it increases above 700 nm. As clear from Fig. 4(b), the reflectance increases as the doping ratio of Cd increases into CZTS thin films.

3.1.1. Analysis of Optical Spectra

To deeply understand the optical properties of CZTS thin films and explore the impact of the doping ratios of Cd, transmittance (T%) spectra of undoped and doped CZTS thin films were used to obtain some fundamental optical properties such as absorption coefficient (α), extinction coefficient (k), optical band gap energy (E_g). The reflectance (R%) spectra were used to determine the refractive index (n).

The absorption coefficient (α) of thin films was obtained using $\alpha = (1/d)ln(1 - R^2/T)$, where T is the s transmittance, R is the reflectance, and d is the thickness of CZTS thin films measured by SEM cross-sections and was almost 500 nm[43,44]. Fig 5 shows the absorption coefficient (α) of undoped CZTS thin film and CZTS thin films doped with different ratios of Cd. The highest values of the absorption coefficient for thin films of CZTS were at wavelengths less than 300 nm, while for wavelengths higher than 300 nm, the absorption coefficient decreases remarkably as the wavelength increases. The absorption coefficient value of undoped CZTS films at the wavelength 550 nm was about $3.6 * 10^4\ cm^{-1}$ and increased up to be about $5 * 10^4\ cm^{-1}$ at the doping ratio 4% of Cd, which was the highest value of α for all prepared thin films.

The extinction coefficient (k) is considered as a measure of light energy loss by absorption and scattering per unit volume and was obtained by $k = \alpha\lambda/4\pi$, where α is absorption coefficient and λ is the wavelength of incident light[45]. Fig 6 shows the extinction coefficient (k) of undoped CZTS thin film and CZTS thin films doped with different ratios of Cd. Generally, the highest values of k were at the absorption edge $\lambda = 300\ nm$, above 300 nm, the extinction coefficient decreases as the wavelength increase, meaning that the electromagnetic waves could pass through the film with less absorption and scattering, and this match the absorption coefficient behavior. The extinction coefficients show increasing due to increasing the concentration of Cd into the thin films, mainly at the 4 % doping ratio, there is a clear rising in k values.

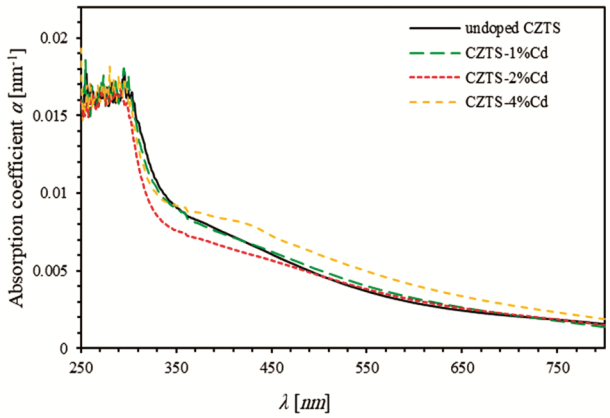

Fig. 5 — Absorption coefficient (α) of undoped CZTS thin films and CZTS doped with different ratios of Cd.

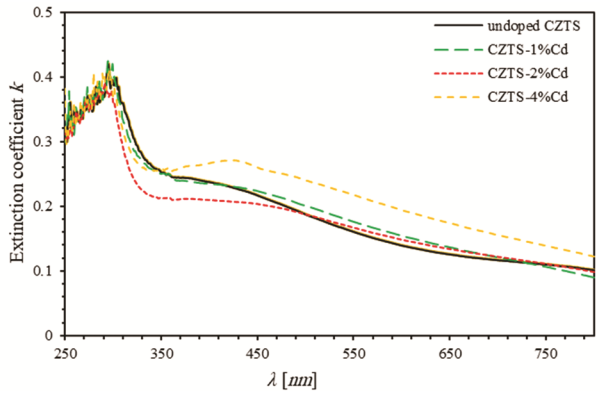

Fig. 6 — Extinction coefficient (k) of undoped CZTS thin films and CZTS doped with different ratios of Cd.

The optical band gap energy (E_g) was determined using transmittance spectra and the absorption spectra of thin films. The relation between the photon energy (hυ), the absorption coefficient (α) , and the bandgap energy can be estimated using the following equation (Tauc plot)[43,46].

$$(\alpha h\upsilon)^{\frac{1}{n}} = A(h\upsilon - E_g) \quad \ldots (4)$$

where A is the band tailing constant and n is the power factor of the transition relies on the nature of thin films (crystal or amorphous), which is equal to ½ for direct transition and 2 for indirect transition if the relation between the $(\alpha h\upsilon)^2$ and the photon energy ($h\upsilon$) is linear. It means that the thin film allows the direct transition, which supports that the CZTS thin films have direct bandgap energy[47].

To determine the optical band gap energy in order to understand the effect of doping ratios of Cd on CZTS thin films, $(\alpha h\upsilon)^2$ versus the photon energy ($h\upsilon$) were plotted. The intercept value gives the bandgap energy assuming α equals to zero.

Fig 7 shows the variation of $(\alpha h\upsilon)^2$ versus photon energy ($h\upsilon$) of undoped CZTS thin film and CZTS thin films doped with (1 %, 2 %, 4 %) of Cd. The direct bandgap energy of undoped CZTS thin film was found to be about 1.594 $eV$and decreased to be about 1.523 eV when the CZTS thin film doped with 4 % of Cd. It is obvious that the optical band gap energy decreases as the doping ratio of Cd increases in CZTS thin films. This reduction in the optical bandgap

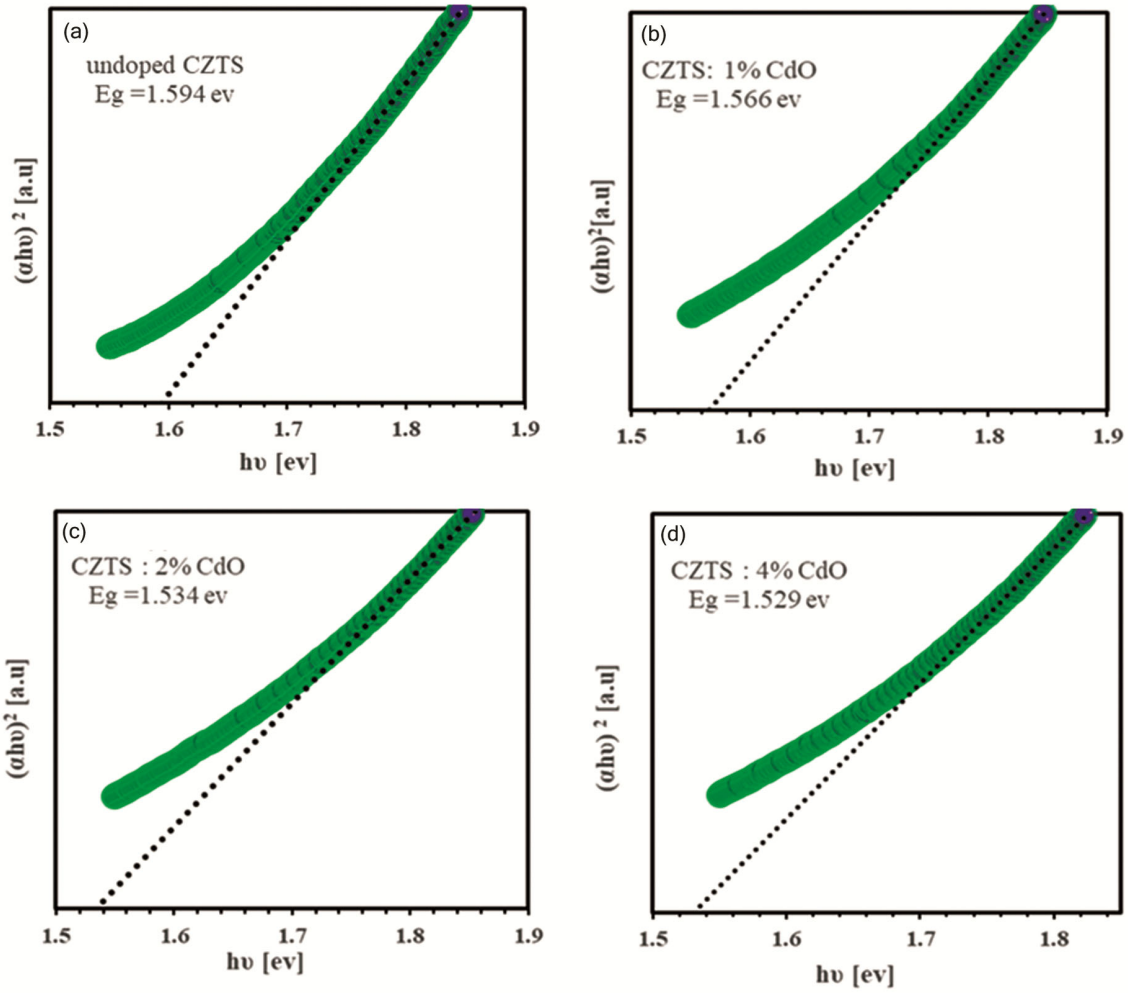

Fig. 7 — Variation of $(\alpha h\upsilon)^2$ versus photon energy $(h\upsilon)$ of a) undoped CZTS thin film and b,c,d) CZTS thin films doped with (1 %, 2 %, 4 %) of Cd, respectively.

energy of thin films may be attributed to the increase in the crystallite size[3], which is consistent with the XRD results that were previously presented in Table 2. Moreover, the obtained optical bandgap energy values almost agree with some previous studies[3,47].

The refractive index (n) is considered as a fundamental optical property for materials used in optoelectronic devices and directly depends on the electronic polarizability of ions in the materials[48]. Determining the refractive index of thin films is very necessary; the refractive index of CZTS thin films has been calculated using the formula; $n = \left(1 + R/1- R\right) + \sqrt{(4R/(1-R^2) - k^2}$, where R is the reflectance value and k is the extinction coefficient[46,49] Fig 8 shows the variation in the refractive index spectra as a function of wavelength of undoped CZTS thin film and CZTS thin films doped with (1 %, 2 %, 4 %) of Cd. In general, the refractive index decreases as λ increases from 250 nm to 700 nm, while it increases above 700 nm. Undoped CZTS thin film has the smallest value of n of about 1.5 and increases up to 1.7 due to doping thin films of CZTS with 4 % of Cd.

3.1.2 Analysis of Refractive index (*n*)

The refractive index values of CZTS thin films have been analyzed by various models to determine different optical parameters, which are contributory in determining the fitness of the materials for use in optical application design and the spectral dispersion devices as well the optical communication[43].

1. Dispersion parameters

The dispersion parameters include the dispersion energy (E_d), effective single oscillator energy (E_0), zero-frequency refractive index (n_0), zero-frequency dielectric (ε_0) , and the optical moments, which could be obtained using Wemple–DiDomenico (WDD) model that has a mathematical form presented in the following formula[40,50-52].

$$(n^2-1)^{-1} = \frac{E_0}{E_d} - \frac{(h\nu)^2}{E_0 E_d} \quad \ldots (4)$$

where n is the refractive index, $h\nu$ is the photon energy, E_d is the dispersive energy, and E_0 is the single oscillator energy[51,53,54].

The dispersion energy E_d expresses the average strength of inter-band optical transitions depending on the internal structure of the material, E_0 gives quantitative information about the total band structure of the material[50]. As shown in Fig 9, $(n^2-1)^{-1}$ as a function of $(h\nu)^2$ was plotted for undoped and doped CZTS thin films to estimate the values of E_d andE_0 via fitting the linear relation. The slope of linear fitting gives $(E_0E_d)^{-1}$ values, while the intercept with the vertical axis gives (E_0/E_d). The oscillation strength parameter (f) was calculated by $f = E_0E_d$ [55]. The values of E_d, E_0 and f for all CZTS thin films (undoped and doped) were tabulated in Table 3. The E_d and E_0 values are

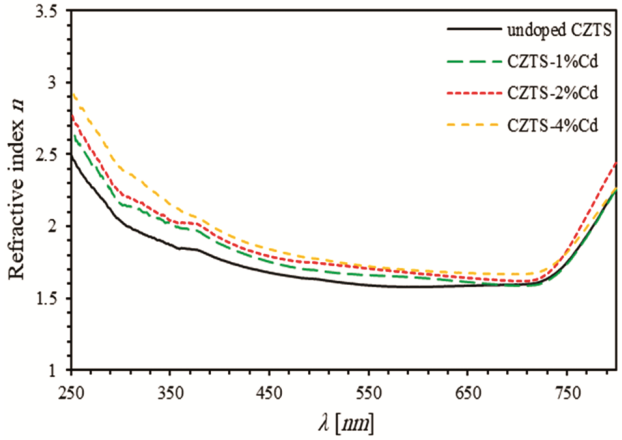

Fig. 8 — Refractive index (n) spectra of wavelength of undoped CZTS thin film and CZTS thin films doped with (1%,2%,4%) of Cd as a function of wavelength.

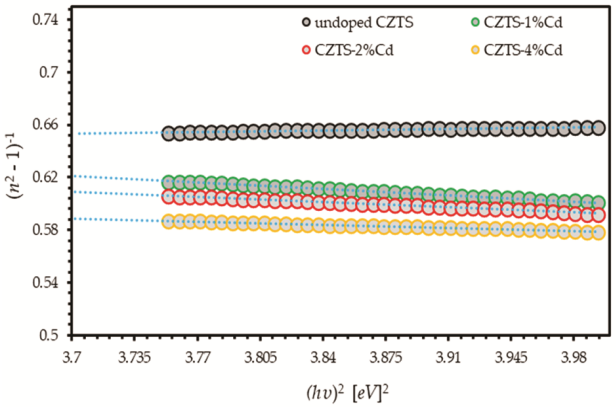

Fig. 9 — Plots of $(n^2-1)^{-1}$ as a function of $(h\nu)^2$ of undoped CZTS thin film and Cd-doped CZTS thin films.

Table 3 — Estimation of some optical parameters of the undoped CZTS, Cd doped CZTS thin films

Parameter	Symbol	undoped CZTS	CZTS-1%Cd	CZTS -2%Cd	CZTS -4%Cd
Effective single oscillator energy $[eV]$	E_0	5.1	5	4.33	4.30
Dispersion energy $[eV]$	E_d	6.95	6.9	5.9	5.7
oscillator strengths $[eV]^2$	f	35.8	35	25.7	24.5
zero-frequency refractive index	n_0	1.53	1.54	1.54	1.52
Zero-frequency dielectric constant	ε_0	2.35	2.37	2.37	2.32
Optical Moments	M_{-1}	1.35	1.37	1.37	1.31
Optical Moments $[eV]^{-2}$	M_{-3}	0.051	0.053	0.073	0.071
Oscillator length strength $*10^{13}[m^{-2}]$	S_0	1.68	1.47	1.8	1.56
Average oscillator wavelength $[nm]$	λ_0	267	288	273	289
High-frequency dielectric	ε	4.8	5.8	6	6.1
Charge carrier density $*10^{27}\,[m^{-3}]$	N_c	2.11	3.15	3.34	3.38
Density of state $*10^{57}\,[m^{-3}/kg]$	(N_c/m^*)	1.16	1.73	1.84	1.86
Plasma frequency $*10^{15}\,[rad/s]$	$_p$	1.9	2.13	2.14	2.15
Relaxation time $*10^{-15}\,[s]$	τ	3.7	5.9	6.3	7.2
Optical mobility $*10^{-3}$	μ_{opt}	1.4	2.3	2.5	2.9
Optical resistivity $*10^{-6}$	ρ_{opt}	2	0.83	0.74	0.63

necessary for the identification of the optical properties for materials that used in designing the spectral dispersion devices and the optical communication function.

The E_d , E_0 and f values of undoped CZTS thin film were found to be about 6.95 eV 5.1 eV and 35.8 eV^2, respectively. It is observed that E_d , E_0 and f values decrease with increasing the Cd concentration into CZTS thin films, where the smallest values were found for 4% Cd-doped CZTS thin film to be about 5.6 eV 4.3 $eV$and 24 eV^2, respectively.

The variation of E_0 values is related to the number of valence electrons per anion as well the coordination number for anion[56]. Both of the oscillation energy E_0 and the optical band gap energy decrease with increasing the doping ratio of Cd.

The obtained values of E_d and E_0 have been employed to estimate each of the zero-frequency refractive index (n_0) and the zero-frequency dielectric constant (ε_0) by equation 6, which represent a special case to Wemple–DiDomenico equation when the incident photon energy $(h\nu)$ is set to be zero[51,55,57].

$$\varepsilon_0 = n_0^2 = 1 + \frac{E_d}{E_0} \quad \ldots (6)$$

The zero-frequency refractive index (n_0) and the zero-frequency dielectric constant (ε_0) of undoped CZTS thin films were found to be about 1.53 and 2.35, respectively. There is a slight variation in the values of n_0 and ε_0 for Cd-doped CZTS thin films, as shown in Table 3. The optical moments M_{-1} and M_{-3} also can be evaluated for undoped and doped CZTS thin films using the following two equations (7) and (8)[52].

$$E_0^2 = \frac{M_{-1}}{M_{-3}} \quad \ldots (7)$$

$$E_d^2 = \frac{M_{-1}^3}{M_{-3}} \quad \ldots (8)$$

The values of M_{-1} and M_{-3} moments for undoped CZTS thin film are estimated to be 1.35 and 0.051 eV^{-2}, respectively. The obtained values are again listed in Table 3.

On the other hand, the Sellmeier model can be employed to estimate the average oscillator strength (S_0) and the average oscillator wavelength (λ_0) parameters and describe the dispersive behavior for undoped and doped CZTS thin films. Sellmeier model represents a relationship between the refractive index (n) and the wavelength of incident light (λ) with each oscillator of strength (S_0) and the average oscillator wavelength (λ_0) as shown in equation 9[46].

$$n^2 - 1 = \frac{S_0\lambda_0^2}{1-(\lambda_0/\lambda)^2} \quad \ldots (9)$$

As shown in Fig 10, $(n^2-1)^{-1}$ as a function of λ^{-2} was plotted for undoped CZTS thin film and Cd-doped CZTS thin films. The slope of linear fitting gives $(S_0)^{-1}$ values while the intercept with the vertical axis gives $(S_0\lambda_0)^{-1}$. The obtained values of S_0 and λ_0 for undoped CZTS thin film were $1.68 * 10^{13}\ m^{-2}$ and 267 nm, respectively. The values of S_0 and λ_0 are also presented in Table 3.

2. High-frequency dielectric constant and density of state

The refractive index spectra can be employed to estimate each density of state N_c/m^* and the high-frequency dielectric constant (ε_∞) using the following formula deduced by Spitzer-Fan (equation 10), while the plasma frequency (ω_p) could be determined by equation 11[48,58,59]

$$n^2 = \varepsilon' = \varepsilon_\infty - \frac{1}{4\pi^2\varepsilon_0}\left(\frac{e^2}{c^2}\right)\left(\frac{N_c}{m^*}\right)\lambda^2 \quad \ldots (10)$$

$$\omega_p^2 = N_c^2/\varepsilon_\omega\varepsilon_0 m^* \quad \ldots \quad \ldots (11)$$

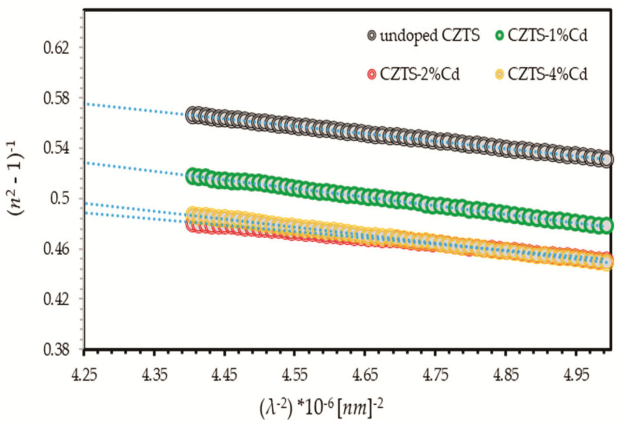

Fig. 10 — Plots of $(n^2-1)^{-1}$ as a function of λ^{-2} of undoped CZTS thin film and Cd-doped CZTS thin films.

where ε' is the real dielectric constant, ε_0 is the dielectric constant of vacuum, ε_∞ is the high-frequency dielectric constant, N_c is the charge carrier density, e is the electronic charge, c is the speed of light in vacuum and m^* is the electron effective mass which is almost equal $0.20m_e$ for CZTS[7]. As shown in Fig 11, n^2 as a function of λ^2 was plotted for undoped CZTS thin film and Cd-doped CZTS thin films. The N_c/m^* values could be determined from the slope of the straight line where the slope gives the value of $\frac{1}{4\pi^2\varepsilon_0}\left(\frac{e^2}{c^2}\right)\left(\frac{N_c}{m^*}\right)$, while $\varepsilon_\square$ values are estimated at λ^2 equal zero. The obtained values were tabulated in Table 3.

The high-frequency dielectric constant (ε_∞), density of state (N_c/m^*) and plasma frequency (ω_p) for undoped CZTS thin film were found as 4.8, $1.16 * 10^{57}\, m^{-3}/kg$ and $1.9 * 10^{15}\, rad/s$, respectively. It was found that the values of ε, N_c/m^* and ω_p increased as the Cd concentration increased, and the maximum values were found to be 6.1, $1.68 * 10^{57}\, m^{-3}/kg$ and $2.15 * 10^{15}\, rad/s$, respectively.

3. Relaxation Time and Optical Resistivity

The imaginary dielectric constant (ε") as a function of the wavelength of the incident photon(λ^3) could be employed to estimate the relaxation time and the optical mobility as well the optical resistivity using the following equations (12), (13) and (14), respectively[46,60].

$$\varepsilon'' = 2nk = \frac{1}{4\pi^3\varepsilon_0}\left(\frac{e^2}{c^3}\right)\left(\frac{N_c}{m^*}\right)\left(\frac{1}{\tau}\right)\lambda^3 \quad \ldots (12)$$

$$\mu_{opt} = (e\tau/m^*) \quad \ldots (13)$$

$$\rho_{opt} = (1/(e\,\mu_{opt}\,N_c)) \quad \ldots (14)$$

where k is the extinction coefficient, τ is the relaxation time, μ_{opt} is the optical mobility and ρ_{opt} is the optical resistivity. As shown in Fig 12, ε" as a function of λ^3 is plotted for undoped CZTS thin film and Cd-doped CZTS thin films to determine the relaxation time via fitting the linear relation, where the relaxation time could be determined from the slope of the straight line and from the obtained values of N_C/m^*.

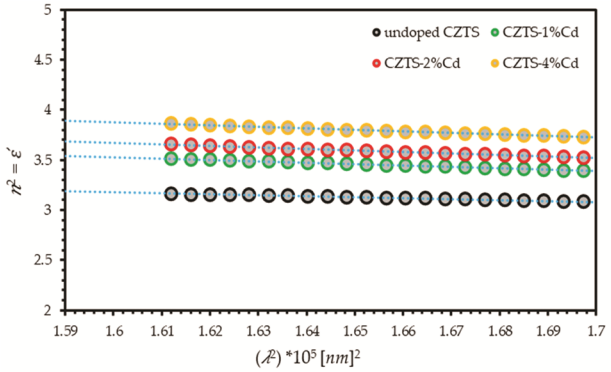

Fig. 11 — Plots of n^2 as a function of λ^2 of undoped CZTS thin film and Cd-doped CZTS thin films.

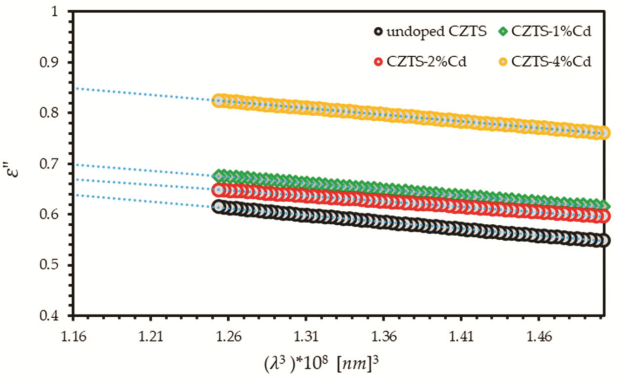

Fig. 12 — Plots of ε" as a function of λ^3 of undoped CZTS thin film and Cd-doped CZTS thin films.

The relaxation time, the optical mobility, and the optical resistivity values for undoped CZTS thin film were found to be $3.7 * 10^{-15}\, s$ and $1.4 * 10^{-3}$ and $2 * 10^{-6}$, respectively. It was observed that the values of the relaxation time and the optical mobility increased to be $7.2 * 10^{-15}\, s$ and $2.9 * 10^{-3}$ as the Cd concentration increased, while the optical resistivity values decreased to be $0.63 * 10^{-6}$. The obtained rustles of τ, μ_{opt} and ρ_{opt} were listed in Table 3.

4 Conclusion.

Nanostructured undoped CZTS thin film and Cd-doped CZTS thin films with doping ratios (1%, 2% and 4%) were successfully fabricated on glass substrates using the sol-gel method by immersion process. The SEM micrographs demonstrated that the particles become clearer and larger due to increasing the doping ratio of Cd into CZTS thin films. The

XRD patterns showed four peaks located at the position 2θ; 28°, 33.4°, 47° and 55° corresponding to the kesterite structure with Miller indices of the crystal reflection plane (112), (200), (220), and (312), respectively. Also, it was observed that there is a small shift in the main peak's (112) position toward lower 2θ values and this shift increased as the Cd concentration increased in CZTS thins due to increasing the (d), which may be attributed to the larger effective ionic radius of Cd^{+2} compared to Cu^{+2} , Zn^{+2} as the small ions replaced with large ions. The average crystal size (D) and the volume of unit cell increase while the average microstrain (ε), crystallites density(N), dislocation density (δ), the total internal stress (σ) as well the strain energy density (E_d) decrease as the Cd concentration increase into CZTS thin films.

Furthermore, the optical band gap energy was found to be 1.59 eV for doped CZTS thin film, and this value decreased to become 1.52 eV for 4% Cd-doped CZTS thin film as well; it was noticed that the absorption (α) and the extinction coefficients (k) increase with increasing the doping ratio. Finally, the refractive index values of CZTS thin films have been analyzed using various models to estimate the dispersion parameters, average oscillator strength (S_0), average oscillator wavelength (λ_0), density of state N_c/m^*, high-frequency dielectric constant (ε_ω), plasma frequency (ω_p), relaxation time (τ) as well optical mobility (μ_{opt}) and optical resistivity (ρ_{opt}). Our results showed that as the Cd atoms increase in the CZTS thin films, there are improvements in the grain size, crystal structure parameters, and the optical band gap energy, which have a significant role in improving the efficiency of the CZTS thin film solar cells.

Acknowledgments

The authors would like to thank Jordan University of Science and Technology in Jordan for the generous financial and technical support provided by the Deanship of Scientific Research. The authors would like to thank Ahmad Ali Ahmad (Omari) in giving unlimited access to use thin films Laboratory, our thanks also for M-Ali Al-Akhras for helping to use his biomedical Laboratory.

References

1 Chen S, Walsh A, Gong X G & Wei S H J A, *Adv Mater*, 25 (2013) 1522.
2 Chang Y, Jialiang H, Kaiwen S, Steve J, Yuanfang Z, Heng S, Aobo P, Mingrui H, Fangyang L & Katja E, *Nat Ener*, 3 (2018) 764.
3 Gi L S, Jongmin K, Suk W H, Yongcheol J, AI I, Pawar S M, Sang K H, Woong J & Sik I H, *Curr App Phys*, 14 (2014) 254.
4 Fouad S S, El Radaf I M, Sharma P & El-Bana M S, *J Alloys Compd*, 757 (2018) 124.
5 Sai G G, Senftle T P & Carter E A, *Chem Mater*, 30 (2018) 4543.
6 Siarhei Z, Shun W T K, Hadke S S, Lie S, Guchhait A, Gao Y, Wong L H, Cheng S, Wang X, Dalapati & Kumar G, *Solar Energy*, 194 (2019) 777.
7 Adachi S, Earth-abundant materials for solar cells: Cu2-II-IV-VI4 semiconductors, John Wiley & Sons, Japan, (2015) 307.
8 Mitzi David B, Gunawan Oki, Todorov Teodor K, Wang Kejia & Guha Supratik, *Sol Energ Mater*, 95 (2011) 1421.
9 Moholkar A V, Shinde S S, Babar A R, Sim K U, Kwon Y B, Rajpure K Y, Patil P S, Bhosale C H & Kim J H, *Solar Energy,* 85 (2011) 1354.
10 Moreno R, Ramirez E A & Guzmán G G, *J Phys: Conf Ser*, 687 (2016) 012041.
11 Lin Y P, Chi Y F, Hsieh T E, Chen Y C & Huang K P, *J Alloys Compd, 654* (2016) 498.
12 Patel M & Ray A, *J Phys D: Appl Phys*, 45 (2012) 445103.
13 Rana T R, Shinde N M & Kim J H, *J Mater Lett*, 162 (2016) 40.
14 Gurav K V, Shin S W, Patil U M, Suryawanshi M P, Pawar S M, Gang M G, Vanalakar S A, Yun J H & Kim J H, *J Alloys Compd*, 631 (2015) 178.
15 Sarswat P K & Free M L, *J Physica Status Solidi*, 208 (2011) 2861.
16 Chung C, Rhee D, Yoo D, Choi M, Heo S C, Kim D & Choi C, J *Ceram Process Res*, 14 (2013) 255.
17 Zhang X, Han M, Zheng X & Zeng Z, *J Sol Energ Mater Sol Cells*, 180 (2018) 118.
18 Hussein H M, Sharifi S & Yazdani A, *J Optik*, 241 (2021) 166975.
19 Riha S C, Parkinson B A & Prieto A L, *J Am Chem Soc*, 133 (2011) 15272.
20 Todorov T K, Tang J, Bag S, Gunawan O, Gokmen T, Zhu Y & Mitzi D B, *J Adv Energ Mater*, 3 (2013) 34.
21 Shadrokh Z, Yazdani A & Eshghi H, *J Semicond Sci Technol*, 31 (2016) 045004.
22 Hussein H M & Yazdani A, *J Mater Sci Semicond Process*, 91 (2019) 58.
23 Kaur K, Arora K, Behzad B, Qiao Q & Kumar M, *J Nanotechnol*, 30 (2018) 065706.
24 Singh O P, Sharma A, Gour K S, Husale S & Singh V N, *J Sol Energ Mater Sol Cells*, 157 (2016) 28.
25 Kuo D H & Wubet W, *J Solid State Chem*, 215 (2014) 122.
26 Sapeli M M I, Ferdaous M T, Shahahmadi S A, Sopian K, Chelvanathan P & Amin N, *J Mater Lett*, 221 (2018) 22.
27 Hussein H M & Yazdani A, *J Res Phys*, 12 (2019) 1586.
28 Fu J, Tian Q, Zhou Z, Kou D, Meng Y, Zhou W & Wu S, *J Chem Mater*, 28 (2016) 5821.
29 Yu X, Ren A, Wang F, Wang C, Zhang J, Wang W, Wu L, Li W, Zeng G & Feng L, *Int J Photoenergy*, 2014 (2014) 1110.

30 Tanaka T, Kawasaki D, Nishio M, Guo Q & Ogawa H, *J Physica Status Solidi C*, 3 (2006) 2844.
31 Sarswat P K, Snure M, Free M L & Tiwari A, *J Thin Solid Films*, 520 (2012) 1694.
32 Weber A, Mainz R, Unold T, Schorr S & Schock H W, *J Physica Status Solidi C*, 6 (2009) 1245.
33 Khalkar A, Lim K S, Yu S M, Patole S P & Yoo J B, *Int J Photoenergy*, 2013 (2013).
34 Kumar Y B K, Babu G S, Bhaskar P U & Raja V S, *J Sol Energ Mater Sol Cells*, 93 (2009) 1230.
35 Seol J S, Lee S Y, Lee J C, Nam H D & Kim K H, *J Sol Energ Mater Sol Cells*, 75 (2003) 155.
36 Lee H L, Issam A M, Belmahi M, Assouar M B, Rinnert H & Alnot M, *J Nanomater*, 2009 (2009).
37 Marzougi M, Rabeh M Ben & Kanzari M, *J Thin Solid Films*, 672 (2019) 41.
38 Özdal T, Chtouki T, Kavak H, Figa V, Guichaoua D, Erguig H & Mysliwiec J S B, *J Inorg Organometall Polym Mater*, 31 (2021) 89.
39 Mostafa M S & Kafashan H, *J Superlatt Microstruct*, 126 (2019) 139.
40 Al-Bataineh Q M, Telfah M, Ahmad A A, Alsaad A M, Qattan I A, Baaziz H, Charifi Zo & Telfah A, *Photonics*, 7 (2020) 112.
41 Akl A A, Mahmoud S A, Al-Shomar S M & Hassanien A S, *J Mater Sci Semicond Process*, 74 (2018) 183.
42 Bilgili O, *J Acta Phys Polonica A*, 136 (2019) 3.
43 Hassanien A S & Akl A A, *J Alloys Compd*, 648 (2015) 280.
44 Demichelis F, Kaniadakis G, Tagliaferro A & Tresso E, *J Appl Opt*, 26 (1987) 1737.
45 Alsaad A M, Al-Bataineh Q M, Ahmad A A, Albataineh Z & Telfah A, *J Optik*, 211 (2020) 164641.
46 Fasasi A Y, Osagie E, Pelemo D, Obiajunwa E, Ajenifuja E, Ajao J, Osinkolu G, Makinde W O & Adeoye A E, *J Am Mater Synth Process*, 3 (2018) 12.
47 Pawar S M, Pawar B S, Moholkar A V, Choi D S, Yun J H, Moon J H, Kolekar S S & Kim J H, *J Electrochim Acta*, 55 (2010) 4057.
48 Dhas C R, Venkatesh R, Sivakumar R, Moses R A & Ezhil S, *J Opt Mater*, 72 (2017) 717.
49 Al-Bataineh Q M, Alsaad A M, Ahmad A A & Al-Sawalmih A, *J Electron Mater*, 48 (2019) 5028.
50 Shaaker H S, Hussain W A & Badran H A, *J Adv Appl Sci Res*, 3 (2012) 2940.
51 Wemple S H & Domenico M, *J Phys Rev B*, 3 (1971) 1338.
52 Oriaku C & Osuwa J N C, *J Non-Oxide Glasses*, 3 (2011) 25.
53 Gupta Yashika & Arun P, *J arXiv preprint arXiv*, 1602 (2016) 00120v1.
54 Wenlong Y, Zhongxiang Z, Bin Y, Yongyuan J, Hao T, Dewei G, Hongguo S & Wen Chen, *J Appl Surf Sci*, 257 (2011) 7221.
55 El R I M, Al-Zahrani H Y S, Fouad S S & El-Bana M S, *J Ceram Int*, 46 (2020) 18778.
56 Hannachi A, Oueslati H, Khemiri N & Kanzari M, *J Opt Mater*, 72 (2017) 702.
57 Shaaban E R, Afify N & El-Taher A, *J Alloys Compd*, 482 (2009) 400.
58 Spitzer W G & Fan H Y, *J Phys Rev*, 106 (1957) 882.
59 Bedia F Z, Bedia A, Maloufi N, Aillerie M, Genty F & Benyouce B, *J Alloys Compd*, 616 (2014) 312.
60 Ahmad A A, Al-Bataineh Q M, Alsaad A M, Samara T O & Miss K A A, Phys B: Condens Matter, 593 (2020) 412263.